

Dual Polarized UWB MIMO Antenna with Elliptical Polarization for Access Point with Very High Isolation Using EBG and MSR

Gnanaharan Irene* and Anbazhagan Rajesh

Abstract—A compact microstrip fed dual polarized Ultra Wide Band (UWB) monopole Multiple Input Multiple Output (MIMO) antenna for access point application in Wireless Body Area Networks (WBAN) is proposed. The antenna is elliptically polarized in the 6 to 10.6 GHz band. The proposed structure possesses high isolation with the introduction of Modified Serpentine Structure (MSS) that behaves as a decoupling unit (DU). To further reduce the coupling and to improve the impedance bandwidth, an Electromagnetic Band Gap (EBG) structure is introduced. The proposed antenna has a wide impedance bandwidth with $S_{11} < -10$ dB in the UWB from 3.1–10.6 GHz and has a high isolation $S_{21} < -25$ dB. The antenna has a fractional bandwidth of 106%. The radiation pattern of the antenna is omnidirectional. The Envelope Correlation Coefficient (ECC) is equal to zero, and the capacity loss is 0.264 which proves the diversity characteristics of the proposed antenna.

1. INTRODUCTION

The widely used technology to transmit digital signals over a wide frequency spectrum with low power and high data rate is the Ultra Wide Band (UWB) technology. The inherent nature of the UWB enables the signals to circumvent obstacles with restricted power. The transmission of UWB signals is as short pulses. Considering an indoor environment, due to the presence of multipath components, there is a shift in the time of arrival of these short pulses. This causes a reduction in the interference and improvement in the accuracy of signal path prediction (considering the angle and distance.) The very fine time resolution enabled by the wideband characteristics of UWB enables the immunity to multipath fading to improve. The robustness against jamming is also improved due to the wideband characteristics of UWB. The time resolution of UWB benefits the health monitoring and real time diagnosis of limbs or post-operative medication by specifically tracking the slight variations in movements [1].

Combining UWB technology with Multiple Input Multiple Output (MIMO) technology grants additional benefits. Enhancement in channel capacity is obtained by utilizing multipath propagation. The perks of using the MIMO technology are enhanced channel capacity and transmission range for the equivalent power requirement [2]. In the literature, most of the UWB MIMO antennas are linearly polarized. The main advantage of the circular polarization (CP) compared to linear polarization is its ability to contend in high reflective, multipath, and line of sight scenarios [3]. The multipath fading environment enhances the CP received signal, and it reduces the effect of the multipath fading on the receiver. The resonant modes which are orthogonal and have almost identical amplitude and phase difference of 90° enable the generation of CP [4]. The access points requires omnidirectional radiation pattern as the antenna has to transmit and receive in all directions.

Pattern and polarization diversity hare exploited using UWB MIMO for access point. The antenna consists of slot radiators each providing directive beams. Isolation is improved to greater than 15 dB using grounded slits [5]. A UWB MIMO antenna is proposed with a circular parasitic element to enhance

Received 17 November 2019, Accepted 11 January 2020, Scheduled 29 January 2020

* Corresponding author: Gnanaharan Irene (irenesuriya@gmail.com).

The authors are with the VIT University, Vellore-632014, India.

isolation. The isolation obtained is greater than 21 dB in the higher band. The Envelope Correlation Coefficient (ECC) between the antenna elements is less than 0.007 [6]. A UWB MIMO antenna is proposed, and the isolation between the antenna elements is improved by using a square slot and an inverse L-shaped strip attached to the ground plane. The isolation is greater than 17 dB, and the ECC is below 0.15 [7].

The CP antennas used for MIMO technology has a large footprint. In [8], an antenna resonates in the 3.1 to 4.8 GHz lower UWB. The isolation between elements is greater than 25 dB. Placing the UWB radiators at the centre of the substrate gives the required impedance bandwidth. In [9], a rectangular corrugated antenna is proposed for the S-band. The efficiency of the antenna is 80%, and the gain is 2.26 dB. The antenna has an axial ratio of 3 dB from 2.5 to 3.5 GHz. A slit is introduced in the ground plane to improve the impedance bandwidth. The edges of the patch are corrugated to get the required CP. In [10], a coplanar waveguide (CPW) fed CP monopole antenna is designed for the Industrial, Scientific and Medical (ISM) and Wireless Local Area Network (WLAN) bands for MIMO applications. The antenna has a -10 dB bandwidth from 2.1 to 8 GHz. The isolation between the elements is greater than 17 dB, and the antenna has a gain of 6 dBi. The slot created in the feed line is used to improve impedance matching. An inverse L-shaped arm is introduced to improve the impedance matching and axial ratio.

There are a number of CP antennas proposed for UWB. In [11], a dual-band CP antenna using meandered lines and an Archimedean spiral structure is proposed for UHF and UWB technologies. This antenna can be used for the IoT technology. The meandered lines gives the Ultra High Frequency (UHF) and UWB technologies. This antenna can be used for the Internet of Things (IoT) technology. The meandered lines give the UHF band and CP while the Archimedean spiral structure gives the UWB. In [12], a CP UWB antenna has been proposed with an axial ratio bandwidth of 7.18 to 10.01 GHz. Changes have been made in the dimensions of the proposed antenna to obtain the desired frequency and CP. The dimensions of the ground plane has also been changes to improve the CP bandwidth. In [13], a circle-shaped antenna with triple sense axial ratio bandwidth is proposed. The peak gain of the antenna is 3.8 dB. The UWB property is obtained by utilizing a compact complementary planar monopole. Multiband CP is obtained by etching a T-shaped slit in the ground plane and a rectangular parasitic stub in the radiator. In [14], a square slot antenna is proposed with a simple topology having an axial ratio from 5 to 10.6 GHz. CP is obtained by introducing inverted-L, inverted-F strips in the ground plane. Although a number of CP antenna designs have been proposed for UWB and MIMO applications, there are no designs combining the two technologies in the literature. The proposed design combines the UWB and MIMO technologies.

This paper presents a compact UWB MIMO antenna. Orthogonal polarization is exploited by placing the antenna elements orthogonally. High isolation is obtained by introducing a meandering serpentine resonator (MSR). Partial ground plane is introduced to maintain the high isolation. The salient features of this design are its compact size, complete coverage in the ultra-wide band, a structure which is planar in nature with extremely low correlation coefficient. The design, optimization, and simulation are done using CST Microwave Studio ver. 2016. The verification of the simulated findings is made possible by modelling the antenna and measuring the findings. The practical implication of the proposed UWB MIMO antenna is as an access point (AP) in Wireless Body Area Networks (WBAN) applications. The design of antenna for WBAN is categorized into three types, namely, off-body antenna design, on-body or body-worn or wearable antennas, and in-body or capsule antenna. Among the classifications, the off-body or AP antenna is of major interest as they transport the user traffic between the on-body antenna, in-body antenna, and the external network. Such antennas have to possess good radiation and isolation characteristics as they communicate over various frequency bands.

2. ANTENNA DESIGN

The antenna is designed on an FR4 substrate with dimensions 29×58 mm² and thickness 1.6 mm. The relative permittivity ϵ_r of the FR4 substrate is 4.4, and the loss tangent $\tan \delta$ is 0.02. The proposed UWB-MIMO antenna meets the advantages of a uni-planar antenna. The electromagnetic simulation software, CST Microwave studio using Finite Integration Technique, is used to design and optimize the antenna structure. The antenna exploits the Koch fractal structure along the sides of the trapezoidal

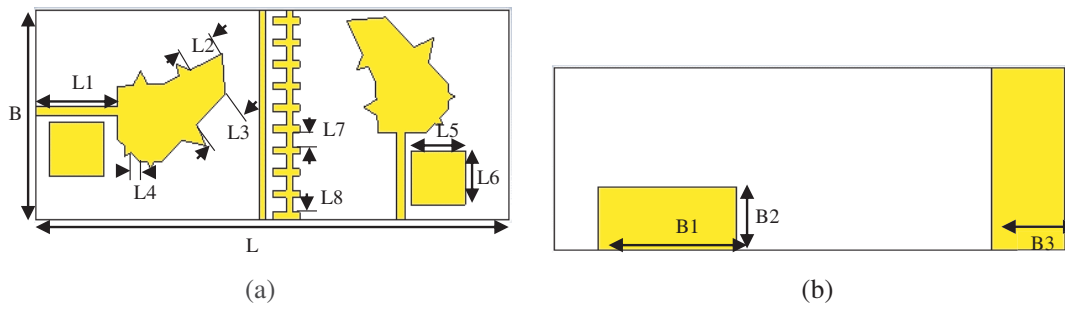


Figure 1. The simulated configuration of the UWB MIMO antenna, (a) the top layer and (b) the bottom layer of the antenna.

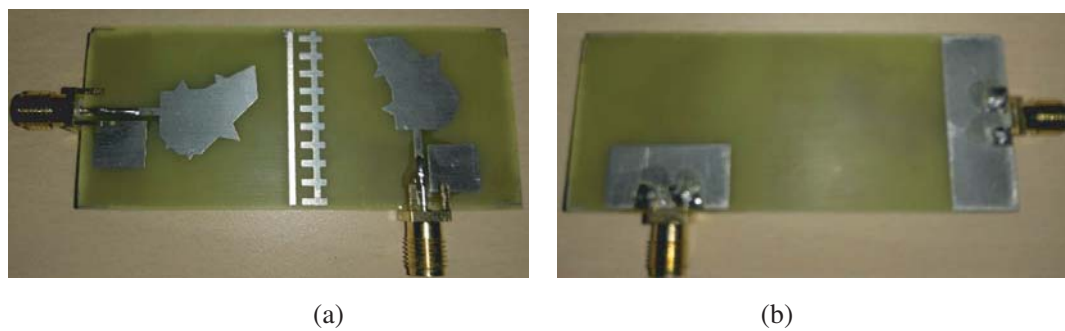


Figure 2. (a) Front view and (b) bottom view of the fabricated antenna.

radiator. Modifications are made in the ground plane which acts as a partial ground plane.

The geometry of the Koch fractal UWB-MIMO antenna is as shown in Fig. 1. The top layer of the UWB-MIMO antenna which consists of two symmetrically placed monopole antenna elements is depicted in Fig. 1(a), and the bottom layer which consists of a partial ground plane is shown in Fig. 1(b). Fig. 2 specifies the fabricated structure of the antenna. Fig. 2(a) specifies the upper layer of the fabricated structure, and Fig. 2(b) specifies the bottom layer of the fabricated structure of the antenna. Microstrip line feeding technique is utilized to feed the antenna elements. Table 1 specifies the parameters of the proposed Access Point UWB MIMO antenna. The simple configuration of the planar monopole antennas provides the advantages of a UWB impedance bandwidth [10].

Table 1. Parameters of the antenna (all dimensions are in mm).

L	B	L_1	L_2	L_3
58	29	12	2.33	2
L_4	L_5	B_1	B_2	B_3
6.63	10	1.2	15	1

The electrical path length increases when the Koch fractal geometry is applied along the trapezoidal monopole. The Koch fractal geometry reduces the resonant frequency, and it can be mathematically represented as a direct function of the limit in the increase of the antennas' effective volume. The application of the Koch fractal geometrical principles induces wideband properties and miniaturization phenomenon. The first iteration of the Koch fractal geometry is applied to the antenna. The Koch fractal geometry is placed along the sides of the monopole, and the iteration is applied to the sides of the monopole to form the Koch fractal monopole antenna.

Parametric optimization is used to satisfy the condition, $|S_{11}| < -10$ dB, and the best structure is determined. The foundational structure of the proposed Access Point UWB MIMO antenna is a trapezoidal monopole. A Koch fractal structure is applied to the sides of the monopole to improve the impedance bandwidth. The antenna elements are placed orthogonally to exploit orthogonal polarization. The Modified Serpentine Structure (MSS) along with the resonator behaves as a Decoupling Unit (DU) and suppresses the surface current between the antenna elements thereby reducing the coupling between the antenna elements. The surface currents from the radiating antenna are captured by the resonating structure which prevents the current from being coupled with the neighbouring antenna.

An MSS improves the isolation between the antenna elements. The DU consists of a combination of modified S structure which can be considered as an MMS and a straight line which resembles a resonator. An Electromagnetic Band Gap (EBG) structure is introduced to further reduce the coupling and widen the impedance bandwidth.

The EBG structure has been introduced to suppress the surface currents between antenna elements. The unique features of the EBG prevent/assist the propagation of the electromagnetic waves in all polarization states and all incident angles in a specified frequency band. There is an improvement in the gain, reduction in the back lobe radiation, and the mutual coupling with the introduction of EBG.

The uni-planar EBG surface is less sensitive for the polarization and incident angle. The significance of the uni-planar EBG is the removal of the vertical vias. This simplifies the fabrication process. The EBG structure suppresses the surface waves, enhances the radiation features of antenna, and reduces the coupling between the antenna elements. The specific absorption ratio is also reduced due to this technique. The other advantage is low cost. The main benefits of the mushroom-like EBG surface are the achievement of a wide-ranging bandwidth and a low frequency. At a certain frequency, the size of the mushroom-like EBG is smaller than the uni-planar EBG.

The centre frequency of the bandgap is determined by

$$\Omega_0 = \frac{1}{\sqrt{LC}}. \quad (1)$$

where L is the inductance, and C is the capacitance

At the resonant frequency, high impedance and in-phase reflection characteristics are attained [11]. To get better performance, the EBG should have a quadratic phase (90°), at the impedance matching frequency.

The evolution of the antenna is shown in Fig. 3. The -10 dB bandwidth for UWB is obtained after the introduction of the DU and EBG structure. The initial structure is trapezoidal monopoles placed orthogonally to exploit orthogonal polarization as depicted in Fig. 3(a). The DU is introduced

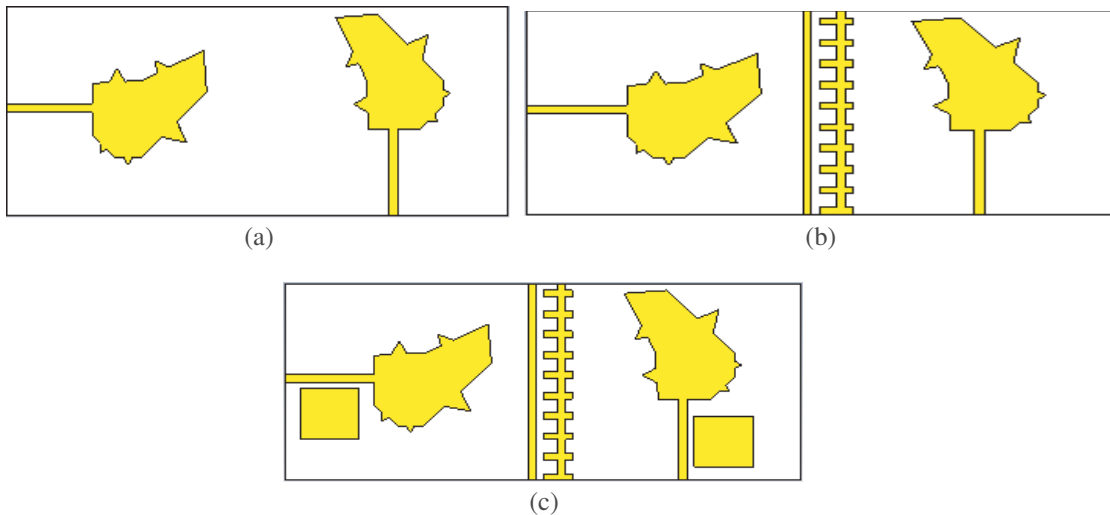


Figure 3. The evolution of the antenna, (a) the trapezoidal monopole placed orthogonally, (b) after the introduction of DU and (c) after the introduction of EBG structure.

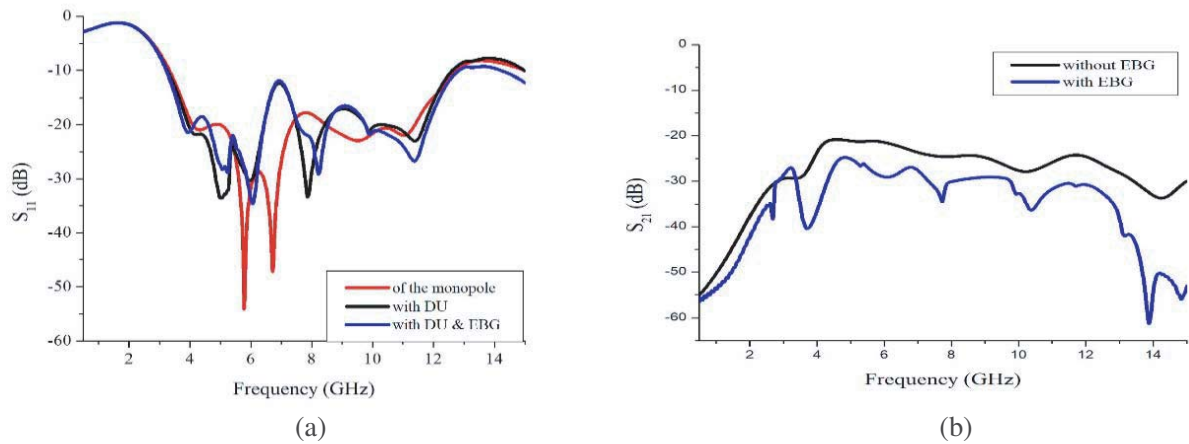


Figure 4. (a) Comparison of S_{11} and (b) comparison of S_{21} of the antenna.

as depicted in Fig. 3(b). This improves the bandwidth of the antenna as depicted in Fig. 4(a). The isolation between the antenna elements is improved by 5 dB as depicted in Fig. 4(b). The EBG structure further improves the bandwidth to the required UWB frequency range as depicted in Fig. 4(a). The S_{11} reflection coefficient obtained as the antenna evolves is as shown in Fig. 4(a). Using a partial ground plane improves the bandwidth of the antenna. The UWB is obtained by combining multiple resonances that are formed within the frequency range from 3.1 to 15 GHz. From the literature, it can be seen that Koch fractal geometry was applied before for obtaining elliptical polarization.

For real input impedance, the total length of the monopole is $\lambda/4$. It is given by

$$L_{strip} = \frac{c}{4f\sqrt{\epsilon_{eff}}} \tag{2}$$

$$\epsilon_{eff} = \frac{\epsilon_r + 1}{2} \tag{3}$$

where ϵ_{eff} is the effective dielectric constant at the resonant frequency f .

The comparison of S_{11} when the antenna is placed symmetrically and when the antenna is placed orthogonally without Koch fractal structure is depicted in Fig. 5. The -10 dB impedance bandwidth for UWB is not satisfied using this method. It can be seen from the Fig. 4(a) that there is an improvement in the impedance bandwidth for the UWB after the introduction of a Koch fractal structure.

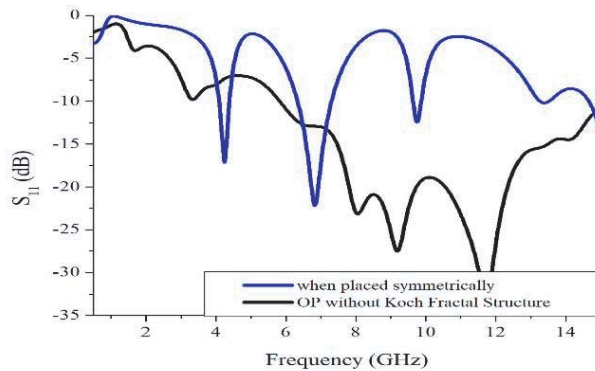


Figure 5. The comparison of the reflection coefficient when the antenna is placed symmetrically and orthogonally polarized without Koch fractal structure.

3. RESULTS AND DISCUSSION

The antenna is fabricated and measured using Vector network analyzer. The comparison of the simulated and measured S_{11} is depicted in Fig. 6(a). It can be seen that the measured result has a 2.34% deviation from the simulated result. This is mainly due to fabrication errors, soldering tolerance, and measurement setup. The comparison of the simulated and measured S_{21} is depicted in Fig. 6(b).

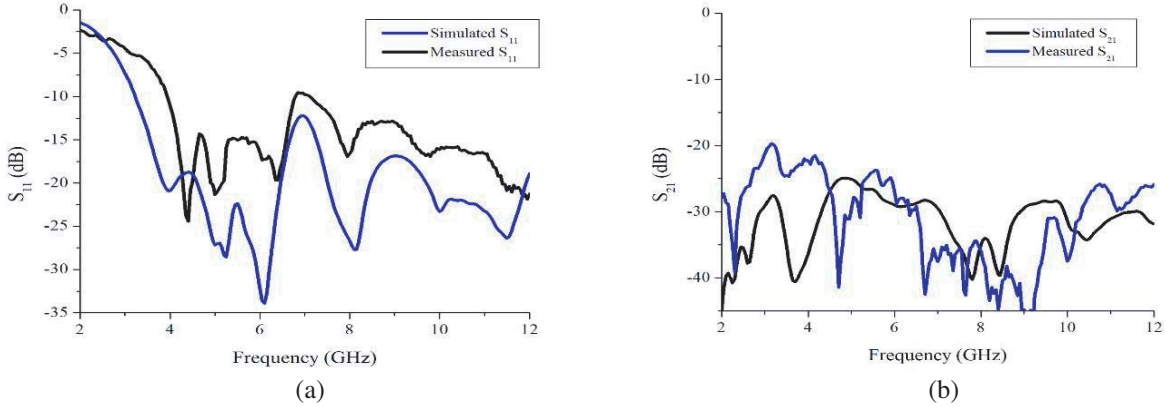


Figure 6. Comparison of the simulated and measured, (a) reflection coefficient and (b) mutual coupling.

3.1. Placement of the DU

A comparison study is done by varying the placement of the DU. It is seen that the -10 dB impedance bandwidth is not obtained for a variation of 5 mm. Fig. 7 represents the comparison of the impedance bandwidths.

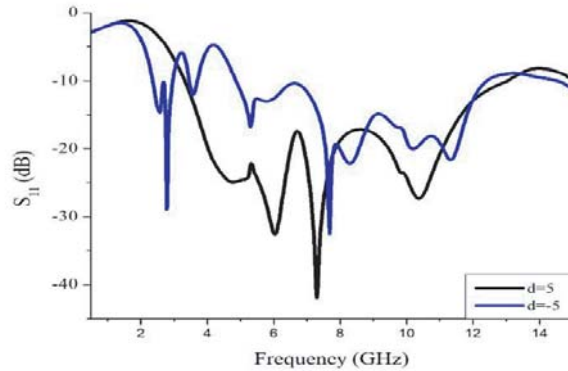


Figure 7. Comparison of the reflection coefficient with shift in the placement of DU.

3.2. Equivalent Circuit of the Antenna

The equivalent circuit gives beneficial comprehension of the performance of the antenna by implementing the foster canonical form without ohmic losses. The large impedance bandwidth is mainly caused by the co-occurrence of various nearby resonances and is specified as parallel RLC networks appended in series [18]. The parallel RLC network is obtained by converting the resonant crests of the input impedance of the UWB antenna. Static antenna capacitance is represented by C_0 , and the probe

inductance is represented by L_0 [18]. Conceptual circuit model is utilized to realize the band notch properties. According to this property, the impedance characteristics at the notched functions are represented by a parallel resonant network or a series R-L-C resonant network [19]. The representation of the real part of the input impedance of S_{11} is given in Fig. 8, and the imaginary part is represented in Fig. 8. From Fig. 8, the representation of the real part suggests that the antenna peaks are at 3.5 GHz, 5.6 GHz, 6.8 GHz, 6.3 GHz, 8.6 GHz, and 9.8 GHz in the UWB, and each frequency is signified as a parallel RLC network connected in series. Fig. 9 represents the equivalent circuit of the proposed Access Point UWB MIMO antenna. The element values of the equivalent circuit are given in Table 2.

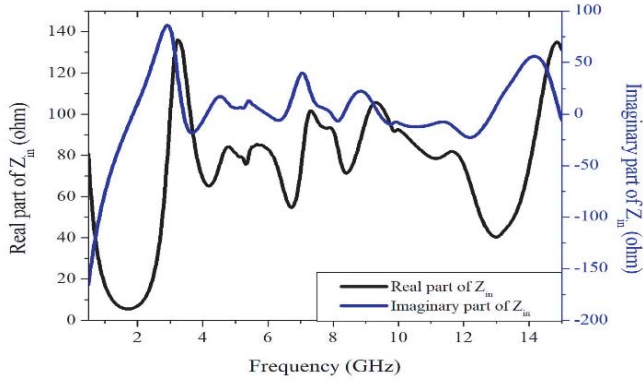


Figure 8. Real part of input impedance of the S_{11} of the antenna.

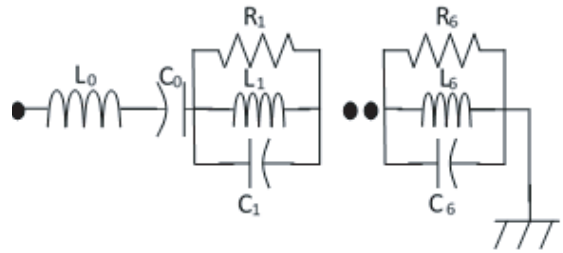


Figure 9. The equivalent circuit of the antenna.

Table 2. Element values of the equivalent circuit of the antenna.

Frequency (GHz)	3.25	4.8	5.73	7.35
R_n (Ω)	135.66	84.17	85.01	101.31
L_n (nH)	1.55	0.345	0.139	0.393
C_n (pF)	1.547	3.186	5.55	1.193
Frequency (GHz)	9.32			
R_n (Ω)	105.67			
L_n (nH)	0.009			
C_n (pF)	0.323			

3.3. Surface Current Distribution

The DU consists of a combination of a modified S structure which can be considered as an MSS and a straight line which resembles a resonator. The meandering of the resonator as seen in MSS increases the electrical path length. The electric field and magnetic field which is transferred amongst the antenna elements is captured by the MSS. This phenomenon of the MSS enables it to behave as a band reject filter having a fundamental frequency which is given by the length. It can be seen from Fig. 10(a) that at 5.23 GHz, there is very little coupling to the neighbouring antenna element when port 1 is excited, and the same result is obtained when port 2 is excited as shown in Fig. 10(b). Fig. 10(c) represents the surface current distribution at 6.08 GHz when port 1 is excited, and Fig. 10(d) is the surface current distribution when port 2 is excited.

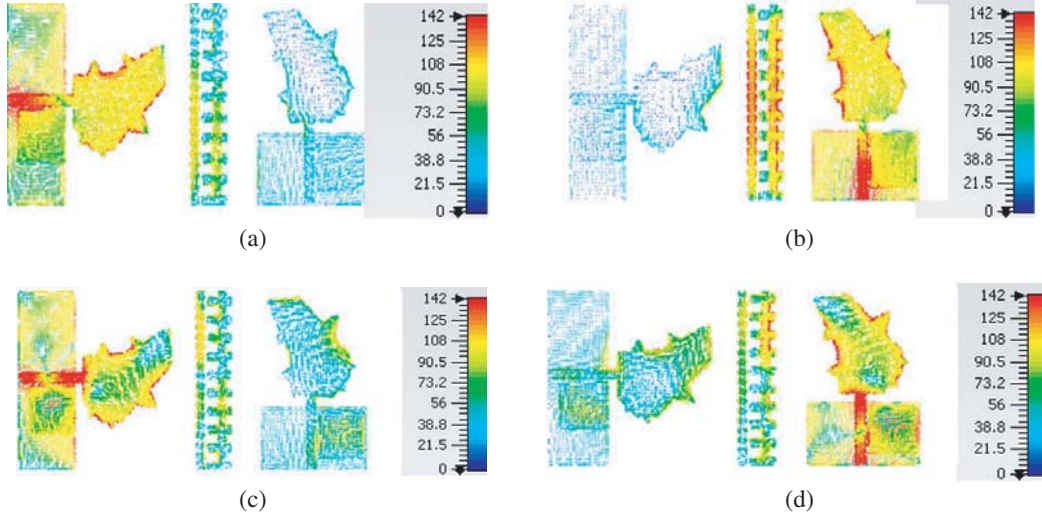


Figure 10. (a) Port 1 at 5.23 GHz, (b) Port 2 at 5.23 GHz, (c) Port 1 at 6.08 GHz and (d) Port 2 at 6.08 GHz.

3.4. Time Domain Characteristics

Considering more performance metrics such as group delay gives better performance results. The delay between the transmitter and receiver should be minimum. Fig. 11 represents the group delay variations which indicates the time domain characteristics of the antenna. The phase of the transfer function is also characterized by the group delay.

3.5. Elliptical Polarization

The antenna is elliptically polarized at 6.5 GHz and at 7.5 GHz. The antenna is elliptically polarized in the span from 9 to 10.6 GHz as indicated in Fig. 12. The introduction of the EBG structure ushers in the above said frequencies. The elliptical polarization is obtained due to the inherent structure of the EBG [16]. As the electromagnetic field component is higher than the other, it creates elliptical polarization.

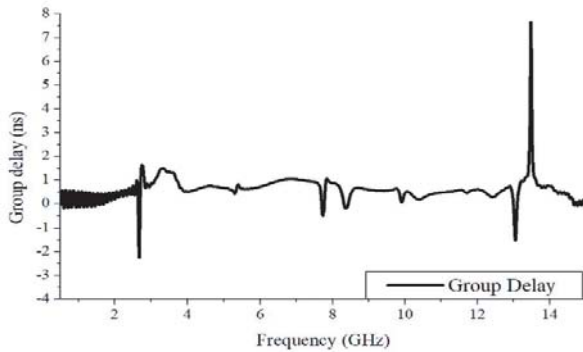


Figure 11. Group delay of the antenna.

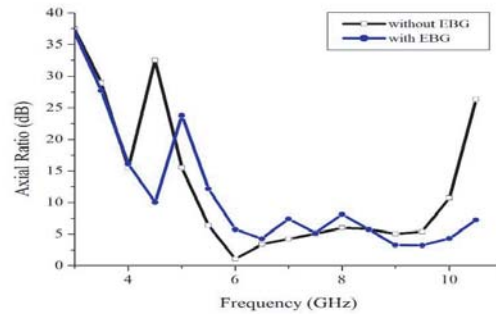


Figure 12. Comparison of the axial ratio owing to the introduction of EBG structure.

The length and width of the EBG are varied to obtain the required elliptical polarization. This creates a slight difference in the amplitudes of the orthogonal components at the resonant modes. The elliptical polarization is considered for the middle and upper bands of UWB as they are free from interferences from other radio frequency bands.

3.6. Radiation Characteristics

The radiation pattern of the antenna at port 1 when port 2 is matched to a $50\ \Omega$ load at the frequencies 5 GHz, 6.1 GHz, and 8.2 GHz is as shown in Fig. 13. The radiation characteristics at 5 GHz in the E plane are as shown in Fig. 13(a), at 6.1 GHz in Fig. 13(b) at 8.2 GHz and in the H plane at 5 GHz is as shown in 13(d), at 6.1 GHz in Fig. 13(e), and at 8.2 GHz as shown in Fig. 13(f). The antenna has an omnidirectional radiation pattern in the E plane and H plane. The simulated radiation pattern is obtained using CST software, and the radiation pattern is measured in an anechoic chamber. There is a huge variation in the E plane at 5 GHz. The variation in the measured and simulated patterns is due to the measurement facilities. The radiation characteristics are enhanced due to the Koch fractal geometry [17]. The gain of the antenna is improved due to the radiation characteristics of the antenna. The gain of the antenna is as shown in Fig. 14. There is a dip in the peak gain at the notch band. The peak gain of the antenna increases due to the introduction of DU and EBG. Although there is a fall in the gain of the antenna at the lower frequencies, the gain of the antenna is 5.8 GHz at 9.5 GHz. This is mainly due to the surface current distribution.

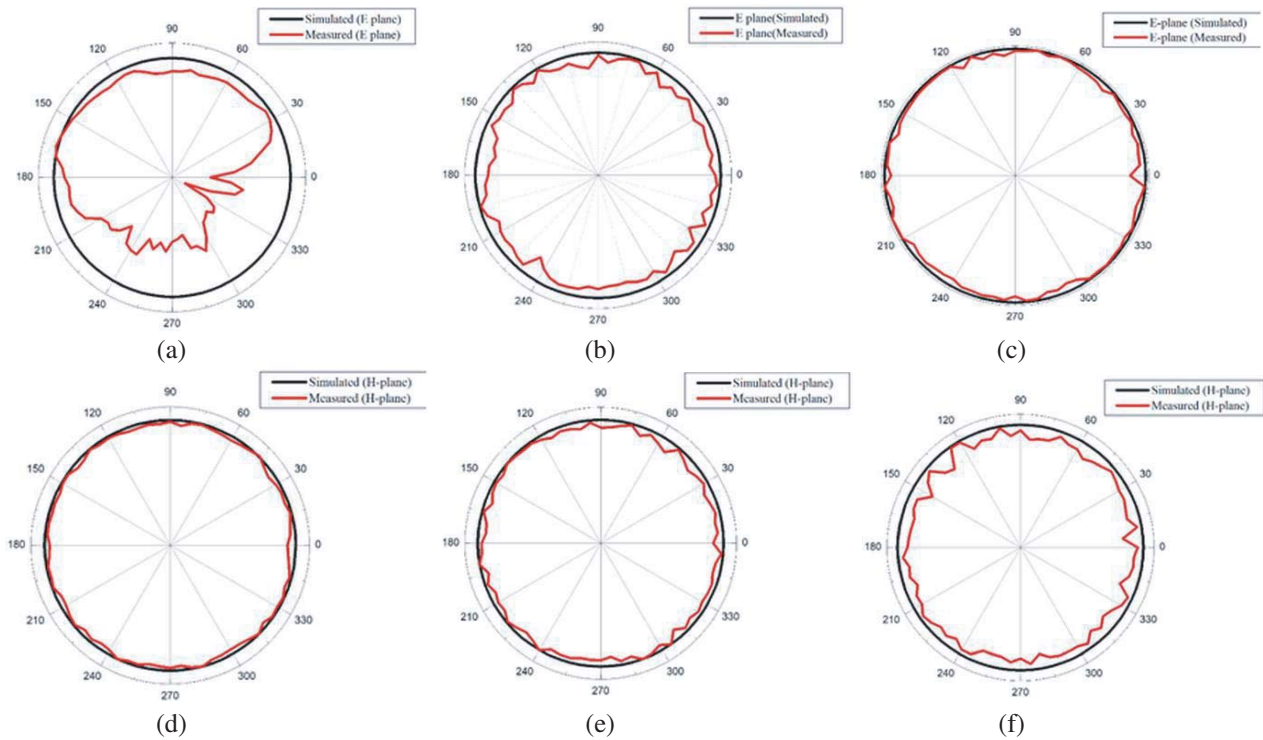


Figure 13. The radiation pattern of the antenna in the E plane at (a) 5 GHz, (b) 6.1 GHz and (c) 8 GHz and in the H plane at (d) 5 GHz, (e) 6.1 GHz and (f) 8 GHz.

Multiplexing efficiency is used to characterize the absolute efficiency of MIMO antennas. The reduction in the power efficiency with respect to an isotropic antenna is represented by multiplexing efficiency.

Figure 15 represents the multiplexing efficiency of the antenna. When the antenna has a uniform 3D angular spectrum and high SNR, the multiplexing is given by,

$$\eta_{MUX} = \sqrt{\left((1 - |\rho_c|^2) \eta_1 \eta_2 \right)} \tag{4}$$

where η_1 and η_2 represent the total efficiency of the initial and second antenna element, respectively, and the envelope correlation coefficient is given by ρ_c .

The multiplexing efficiency of the antenna varies between 88% and 65% in the bands of interest as

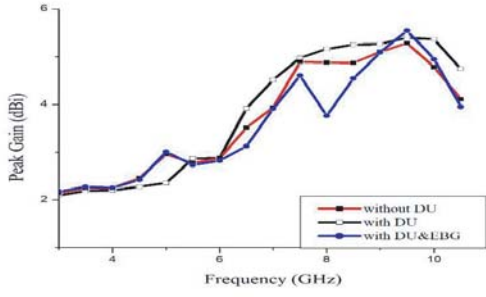


Figure 14. Comparison of the peak gain of the antenna along its process of evolution.

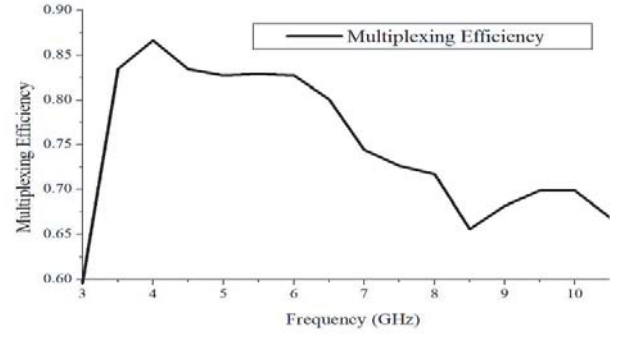


Figure 15. The multiplexing efficiency of the antenna.

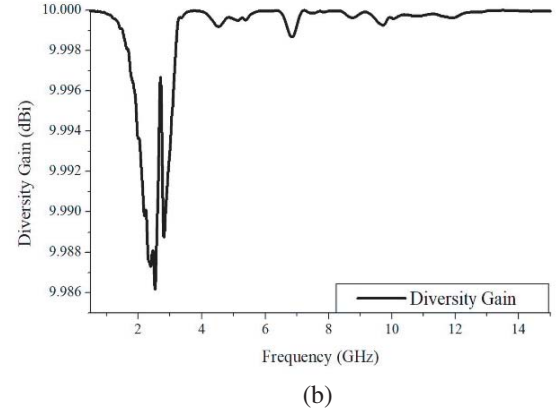
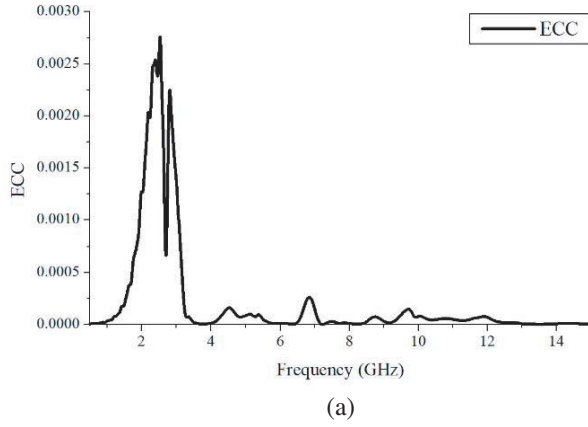


Figure 16. (a) The ECC and (b) Diversity gain of the antenna.

shown in Fig. 15. The lower frequency band of the UWB enjoys greater efficiency than the higher band. The efficiency of the antenna due to linear polarization is higher than that due to elliptical polarization.

3.7. Diversity Characteristics

The two qualities envelope correlation coefficient (ECC) and diversity gain (DG) are used to characterize the diversity performance. When the propagating environment is uniform, the ECC is evaluated as [15].

$$\rho_e = \frac{\left| \iint_{4\pi} [\bar{F}1(\theta, \varphi) * \bar{F}2(\theta, \varphi)] d\Omega \right|^2}{\iint_{4\pi} |\bar{F}1(\theta, \varphi)|^2 d\Omega \iint_{4\pi} |\bar{F}2(\theta, \varphi)|^2 d\Omega} \quad (5)$$

Figure 16(a) depicts the ECC of the proposed UWB-MIMO antenna, which is equal to zero implying good diversity performance.

There is a close tradeoff between diversity gain and ECC. The lower the ECC is, higher the DG is [13]

$$DG = \sqrt{1 - \rho_e} \quad (6)$$

The capacity of the channel seen in a predefined wireless environment is evaluated as a function of the channel environment and the radiation characteristics of the antenna elements. The capacity loss of the proposed UWB MIMO antenna is 0.264.

$$C = \log_2 \left[\det \left(I_N + \frac{\rho}{N} H H^T \right) \right] \quad (7)$$

From Fig. 16(b) it can be observed that the diversity gain remains stable at 10 dBi depicting very good diversity performance. A comparison of the antenna with the literature is given in Table 3. The excellent diversity characteristics enable the antenna to be utilized in a MIMO environment in a WBAN.

Table 3. Comparison of the proposed UWB MIMO antenna with literature.

Parameters	[20]	[21]	[22]	[23]	This Work
Dimensions (mm ²)	45 × 45	40 × 25	48 × 25	40 × 25	58 × 29
Band width (GHz)	2 to 10.6	3.1 to 10.6	3.1 to 10.6	3.1 to 10.6	3.1 to 10.6
Return loss (dB)	-28	-49	-17	-38	-35
Isolation (dB)	< -17	< -15	< -20	< -15	< -27
ECC	0	-	-	< 0.01	0
Gain (dBi)	5	5	-	-	5.8

4. CONCLUSION

A novel, compact and planar UWB-MIMO antenna has been designed and developed. The antenna combines UWB and MIMO technologies to provide very high diversity performance for access point applications. The access point can be used in a WBAN. The antenna covers the entire UWB and has very high isolation. The unavoidable mutual coupling is suppressed by using a Decoupling Unit consisting of an MSS and a reflector. The antenna has an omnidirectional radiation pattern, elliptical polarization characteristics, and excellent diversity characteristics. The significant features of the antenna make it a good candidate for access point application for WBAN.

REFERENCES

1. Abbasi, Q. H., A. Sani, A. Alomainy, and Y. Hao, "Numerical characterization and modeling of subject-specific ultrawideband body-centric radio channels and systems for healthcare applications," *IEEE Transactions on Information Technology in Biomedicine*, Vol. 16, No. 2, 221–227, 2012.
2. Sipal, D., M. P. Abegaonkar, and S. K. Koul, "Easily extendable compact planar UWB MIMO antenna array," *IEEE Antennas Wirel. Propag. Lett.*, Vol. 16, 2328–2331, 2017.
3. Saxena, S., B. K. Kanaujia, S. Dwari, S. Kumar, and R. Tiwari, "A compact microstrip fed dual polarised multiband antenna for IEEE 802.11 a/b/g/n/ac/ax applications," *AEU-International Journal of Electronics and Communications*, Vol. 72, 95–103, 2017.
4. Rahim, S. A., S. Danesh, U. A. Okonkwo, M. Sabran, and M. Khalily, "UWB monopole antenna with circular polarization," *Microwave and Optical Technology Letters*, Vol. 54, No. 4, 949–953, 2012.
5. Mathur, R. and D. Santanu, "8-port multibeam planar UWB-MIMO antenna with pattern and polarisation diversity," *IET Microwaves, Antennas & Propagation*, Vol. 13, No. 13, 2297–2302, 2019.
6. Ghimire, J., K.-W. Choi, and D.-Y. Choi, "Bandwidth enhancement and mutual coupling reduction using a notch and a parasitic structure in a UWB-MIMO antenna," *International Journal of Antennas and Propagation*, Vol. 2019, No. 5, 1–9, 2019.
7. Thakur, E., N. Jaglan, and S. D. Gupta, "Design of compact UWB MIMO antenna with enhanced bandwidth," *Progress In Electromagnetics Research C*, Vol. 97, 83–94, 2019.
8. Zhang, J. and Z. Shen, "Dual-band shared-aperture UHF/UWB RFID reader antenna of circular polarization," *IEEE Transactions on Antennas and Propagation*, Vol. 66, No. 8, 3886–3893, 2018.

9. Nikhare, N. P., P. N. Shinde, and J. P. Shinde, "Circularly polarized MIMO monopole antenna with Defected Ground Structure for S-band application," *2016 International Conference on Computing Communication Control and automation (ICCUBEA)*, 1–4, IEEE, 2016.
10. Haghparast, A. H. and G. Dadashzadeh, "A dual band polygon shaped CPW-fed planar monopole antenna with circular polarization and isolation enhancement for MIMO applications," *2015 9th European Conference on Antennas and Propagation (EuCAP)*, 1–4, IEEE, 2015.
11. Gao, X. and Z. Shen, "UHF/UWB tag antenna of circular polarization," *IEEE Transactions on Antennas and Propagation*, Vol 64, No. 9, 3794–3802, 2016.
12. Rahim, S. A., S. Danesh, U. A. Okonkwo, M. Sabran, and M. Khalily, "UWB monopole antenna with circular polarization," *Microwave and Optical Technology Letters*, Vol. 54, No. 4, 949–953, 2012.
13. Li, G., H. Zhai, T. Li, L. Li, and C. Liang, "A compact ultra wideband antenna with triple-sense circular polarization," *2013 Proceedings of the International Symposium on Antennas & Propagation*, Vol. 1, 531–534, IEEE, 2013.
14. El-Hameed, A. S. A., D. A. Salem, E. A. Abdallah, and E. A. Hashish, "Ultra wide band cpw-fed circularly polarized square slot antenna," *2013 IEEE Antennas and Propagation Society International Symposium (APSURSI)*, 3–4, IEEE, 2013.
15. Gulam Nabi Alsath, M. and M. Kanagasabai, "Compact UWB monopole antenna for automotive communications," *IEEE Transactions on Antennas and Propagation*, Vol. 63, No. 9, 4204–4208, 2015.
16. Diblanc, M., E. Rodes, E. Arnaud, M. Thevenot, T. Monediere, and B. Jecko, "Circularly polarized metallic EBG antenna," *IEEE Microwave and Wireless Components Letters*, Vol. 15, No. 10, 638–640, 2005.
17. Puente, C., J. Romeu, R. Pous, J. Ramis, and A. Hijazo, "Small but long Koch fractal monopole," *Electronics Letters*, Vol. 34, No. 1, 9–10, 1998.
18. Pele, I., A. Chousseaud, and S. Toutain, "Simultaneous modeling of impedance and radiation pattern antenna for UWB pulse modulation," *Antennas and Propagation Society International Symposium, 2004. IEEE*, Vol. 2, 1871–1874, IEEE, 2004.
19. Zhou, H.-J., B.-H. Sun, Q.-Z. Liu, and J.-Y. Deng, "Implementation and investigation of U-shaped aperture UWB antenna with dual band-notched characteristics," *Electronics Letters*, Vol. 44, No. 24, No. 1, 387–1388, 2008.
20. Shrivishal, T., A. Mohan, and S. Yadav, "A compact Koch fractal UWB MIMO antenna with WLAN band-rejection," *IEEE Antennas and Wireless Propagation Letters*, Vol. 14, 1565–1568, 2015.
21. Shrivishal, T., A. Mohan, and S. Yadav, "A compact octagonal shaped fractal UWB MIMO antenna with 5.5 GHz band-notch characteristics," *IEEE International Microwave and RF Conference (IMaRC)*, 178–181, IEEE, 2014.
22. Zhang, J.-Y., F. Zhang, W.-P. Tian, and Y.-L. Luo, "ACS-fed UWB-MIMO antenna with shared radiator," *Electronics Letters*, Vol. 51, No. 17, 1301–130, 2015.
23. Luo, C.-M., J.-S. Hong, and L.-L. Zhong, "Isolation enhancement of a very compact UWB-MIMO slot antenna with two defected ground structures," *IEEE Antennas and Wireless Propagation Letters*, Vol. 14, 1766–1769, 2015.